Experimental study on the extension of nodal aberration theory to pupil-offset off-axis three-mirror anastigmatic telescopes

Guohao Ju
Hongcai Ma
Zhiyuan Gu
Changxiang Yan

Experimental study on the extension of nodal aberration theory to pupil-offset off-axis three-mirror anastigmatic telescopes

Guohao Ju, * **Hongcai Ma, Zhiyuan Gu, and Changxiang Yan**
Chinese Academy of Science, Changchun Institute of Optics, Fine Mechanics and Physics, Changchun, China

Abstract. The aberration fields of misaligned on-axis telescopes can be described by nodal aberration theory. However, traditional nodal aberration theory cannot directly apply to pupil-offset off-axis systems. In our previous work, the net aberration fields of pupil-offset off-axis two-mirror astronomical telescopes induced by lateral misalignments were investigated by extending nodal aberration theory to include pupil-offset off-axis telescopes with a system-level pupil coordinate transformation through simulation. An experimental study on the net aberration fields of pupil-offset off-axis three-mirror anastigmatic (TMA) telescopes induced by lateral misalignments is further presented. Specifically, the astigmatism and coma aberration fields as well as their inherent relations are analytically expressed, simulated, and quantitatively validated with a real pupil-offset off-axis TMA telescope. Meanwhile, the differences between the aberration fields of misaligned off-axis and on-axis TMA telescopes are revealed and explicated. Our work not only contributes to a deep understanding of the net aberration fields of pupil-offset off-axis TMA telescopes induced by lateral misalignments but also represent an important validation for the extension of nodal aberration theory to pupil-offset off-axis telescopes. © *The Authors. Published by SPIE under a Creative Commons Attribution 4.0 Unported License. Distribution or reproduction of this work in whole or in part requires full attribution of the original publication, including its DOI.* [DOI: 10.1117/1.JATIS.5.2.029001]

Keywords: aberration fields; off-axis three-mirror anastigmatic telescopes; lateral misalignments; nodal aberration theory.

Paper 18030 received May 17, 2018; accepted for publication Mar. 18, 2019; published online Apr. 9, 2019.

1 Introduction

Nodal aberration theory has been a powerful tool in studying the aberration behavior of on-axis optical systems that contain misaligned, or intentionally tilted and/or decentered components.[1,2] This theory develops from the wave aberration theory of Hopkins,[3] based on the concept of shifted aberration field center attributed to Buchroeder[4] and the vector multiplication developed by Shack and Thompson[5] (it is later discovered that the operation had existed in the mathematical literature for about a century).[6,7] Thompson[8–12] developed the concept of nodal aberration theory and further extended this theory to fifth order. This theory was extended to study optical systems with plane symmetry.[13] It was also used to design off-axis optical systems, where the mirrors are tilted to obtain an unobscured configuration.[14,15] This theory was further extended to analytically express the effects of freeform surfaces on the net aberration fields several years ago.[16,17] Recently, the correctness of nodal aberration theory was verified through experiment with a Ritchey–Chrétien telescope.[18]

However, the net aberration field characteristics of off-axis telescopes with an offset pupil induced by misalignments are very different from those of on-axis telescopes. Traditional nodal aberration theory cannot directly apply to pupil-offset off-axis systems. Traditional nodal aberration theory is only directly applicable to optical systems with individually rotationally symmetric surfaces, which can be decentered or tip-tilted, while the surfaces in pupil-offset optical systems are no longer rotationally symmetric. While some discussions have been proposed to give a better understanding of the aberration fields of

pupil-offset off-axis telescopes with lateral, axial, and rotational misalignments,[19–21] the misalignment-induced aberration field characteristics of pupil-offset off-axis telescopes are still not well-known in the area of optics, especially for the case of pupil-offset off-axis three-mirror anastigmatic (TMA) telescopes. In addition, these investigations lacked enough validation through real experiment, which is an impediment to the extension of nodal aberration theory to pupil-offset off-axis telescopes.

In this paper, an experimental study is presented on the net aberration fields (mainly including astigmatism and coma) of pupil-offset off-axis TMA telescopes induced by lateral misalignments. A system-level pupil coordinate transformation is utilized to extend nodal aberration theory to include pupil-offset off-axis systems. The astigmatism and coma aberration fields as well as their inherent relations are analytically studied, simulated, and quantitatively validated with an experiment. It will be shown that the net astigmatic aberration field in the pupil-offset off-axis TMA telescopes induced by lateral misalignments can be seen as a combination of a field-linear component and a larger field-constant component. The field-linear component is nearly the same as the astigmatism that exists in misaligned on-axis TMA telescopes. The field-constant component is mainly attributed to the effects of pupil offset, which converts the misalignment-induced coma in the on-axis parent system to the astigmatism in pupil-offset off-axis system. Due to this effect of pupil offset, the field-constant astigmatic term has inherent relationships with misalignment-induced field-constant coma in pupil-offset off-axis TMA telescopes, which is still field constant. All these results will be verified with a real pupil-offset off-axis TMA telescopes. This work will contribute to a deep understanding of the net aberration fields of pupil-offset

*Address all correspondence to Guohao Ju, E-mail: juguohao123@163.com

off-axis TMA telescopes induced by lateral misalignments. In the following sections, when we refer to an "off-axis system," we particularly mean one in which the "parent" design has a single axis of rotational symmetry, but the entrance pupil is shifted sufficiently that the resulting system is unobscured. We do not discuss those in which the mirrors are tilted to obtain an unobscured configuration and no common axis exists.

This paper is organized as follows. In Sec. 2, the analytic expressions of misalignment-induced astigmatic and coma aberration fields of pupil-offset off-axis TMA telescope are derived under some approximations. In Sec. 3, simulations and some relevant discussions are presented to demonstrate the specific astigmatic and coma aberration fields, including their inherent relationships. The quantitative experimental validation is presented in Sec. 4. The paper is concluded in Sec. 5.

2 Analytic Expressions

The net image plane aberration of rotationally symmetric optical systems consists of the sum of all the individual surface contributions, which can be described by the wave aberration expansion. The wave aberration expansion originally described by Hopkins[3] can be rewritten in vector form as[9]

$$W = \sum_j \sum_p^\infty \sum_n^\infty \sum_m^\infty W_{klmj} (\vec{H} \cdot \vec{H})^p (\vec{\rho} \cdot \vec{\rho})^n (\vec{H} \cdot \vec{\rho})^m, \quad (1)$$

where $k = 2p + m$, $l = 2n + m$, $\vec{H}$ is the normalized field vector, $\vec{\rho}$ is the normalized pupil vector, and W_{klmj} denotes the aberration coefficient for a particular aberration type of surface j.

In the presence of misalignments, the total aberration of the system is still the sum of all the individual surface contributions. However, the center of the aberration field contribution associated with each surface will deviate from the field center in the image. In this case, the aberration function of the system should be modified as

$$W = \sum_j \sum_p^\infty \sum_n^\infty \sum_m^\infty W_{klmj} (\vec{H}_{Aj} \cdot \vec{H}_{Aj})^p (\vec{H}_{Aj} \cdot \vec{\rho})^m (\vec{\rho} \cdot \vec{\rho})^n, \quad (2)$$

with

$$\vec{H}_{Aj} = \vec{H} - \vec{\sigma}_j, \quad (3)$$

where $\vec{H}_{Aj}$ represents the effective field height of surface j, as shown in Fig. 1(a), and $\vec{\sigma}_j$ represents the position of shifted aberration field center of this surface, which is linearly correlated with misalignments of the system.[5,6,22]

Conceptually, an off-axis telescope with lateral misalignments can be obtained by decentering the pupil of a parent on-axis system with the same misalignments while the other elements of the system stay unchanged. The coordinate transformation between the off-axis pupil and on-axis parent pupil can be expressed as[23]

$$\vec{\rho} = \vec{\rho}\,' + \vec{s}, \quad (4)$$

where $\vec{\rho}\,'$ represents the normalized off-axis pupil vector, as shown in Fig. 1(b), and $\vec{s}$ represents the location of the off-axis pupil with reference to on-axis parent pupil.
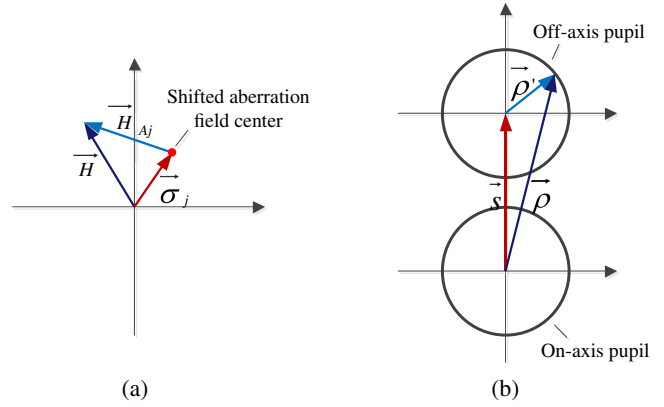

Fig. 1 Illustrations of (a) the effective field height and shifted aberration field center for surface j and (b) the system-level coordinate transformation between on-axis pupil and off-axis pupil.

The aberration function of off-axis systems with lateral misalignments can then be obtained by substituting Eq. (4) into Eq. (2), i.e.,

$$W = \sum_j \sum_p^\infty \sum_n^\infty \sum_m^\infty W_{klmj} (\vec{H}_{Aj} \cdot \vec{H}_{Aj})^p$$
$$\times [\vec{H}_{Aj} \cdot (\vec{\rho}\,' + \vec{s})]^m [(\vec{\rho}\,' + \vec{s}) \cdot (\vec{\rho}\,' + \vec{s})]^n. \quad (5)$$

It can be seen that the aberration function of the off-axis system has been expressed with the normalized pupil vector of this off-axis system.

Before analyzing the misalignment-induced aberration field characteristics of off-axis systems, we should explicitly express the field dependencies of different aberration types. To this end, Eq. (5) should be rewritten as[19]

$$W = \sum_n^\infty \sum_m^\infty \vec{C}_{lm} \cdot [\vec{\rho}^n (\vec{\rho} \cdot \vec{\rho})^m], \quad (6)$$

where $l = 2n + m$ and $\vec{C}_{lm}$ represents the coefficient of certain aberration type at certain field point. The primes in Eq. (6) have been neglected. Here, $\vec{C}_{lm}$ can further be divided into the following three components:

$$\vec{C}_{lm} = \vec{C}_{lm}^{(0)}(\vec{H}, \vec{s}) + \vec{C}_{lm}^{(1)}(\vec{H}, \vec{s}, \vec{\sigma}_1, \vec{\sigma}_2, ..)$$
$$+ \sum_{i=2}^\infty \vec{C}_{lm}^{(i)}(\vec{H}, \vec{s}, \vec{\sigma}_1, \vec{\sigma}_2, ..), \quad (7)$$

where $\vec{C}_{lm}^{(0)}(\vec{H}, \vec{s})$ represents the aberration component for the nominal off-axis system, which is independent of misalignments, $\vec{C}_{lm}^{(1)}(\vec{H}, \vec{s}, \vec{\sigma}_1, \vec{\sigma}_2, ..)$ represents the aberration component linearly related to misalignments, and the other one represents the sum of the aberration components, which have higher-order (≥ 2) misalignment dependence. When only the third-order aberrations of the on-axis parent telescope are considered, the specific expressions of $\vec{C}_{lm}^{(0)}$, $\vec{C}_{lm}^{(1)}$, and $\sum_{i=2}^\infty \vec{C}_{lm}^{(i)}$ are shown in Table 1, and the derivations for these expressions are presented in Appendix A.

The tip–tilt term ($\vec{C}_{11} \cdot \vec{\rho}$) that does not affect imaging quality is not considered in Table 1, and the expression of $\vec{A}_{klm}$ is

Table 1 The specific expressions of $\vec{C}_{lm}^{(0)}$, $\vec{C}_{lm}^{(1)}$, and $\sum_{i=2}^{\infty} \vec{C}_{lm}^{(i)}$ for different aberration types.

Aberration type	$\vec{C}_{lm}^{(0)}$	$\vec{C}_{lm}^{(1)}$	$\sum_{i=2}^{\infty} \vec{C}_{lm}^{(i)}$
$\vec{C}_{20} \cdot (\vec{\rho} \cdot \vec{\rho})$	$W_{020} + W_{220M}(\vec{H} \cdot \vec{H}) + 2W_{131}(\vec{s} \cdot \vec{H}) + 4W_{040}(\vec{s} \cdot \vec{s})$	$-2\vec{A}_{220M} \cdot \vec{H} - 2\vec{A}_{131} \cdot \vec{s}$	$\sum_j W_{220M}(\vec{\sigma}_j \cdot \vec{\sigma}_j)$
$\vec{C}_{22} \cdot \vec{\rho}^2$	$\frac{1}{2} W_{222}\vec{H}^2 + W_{131}\vec{s}\vec{H} + 2W_{040}\vec{s}^2$	$-\vec{A}_{222}\vec{H} - \vec{A}_{131}\vec{s}$	$\sum_j W_{222}\vec{\sigma}_j^2$
$\vec{C}_{31} \cdot \vec{\rho}(\vec{\rho} \cdot \vec{\rho})$	$W_{131}\vec{H} + 4W_{040}\vec{s}$	$-\vec{A}_{131}$	0
$\vec{C}_{40} \cdot (\vec{\rho} \cdot \vec{\rho})^2$	W_{040}	0	0

$$\vec{A}_{klm} = \sum_j W_{klm}\vec{\sigma}_j. \qquad (8)$$

When only the third-order aberrations of the on-axis parent system are considered, $\vec{C}_{lm}^{(i)}$ ($i > 2$) is not existed.

In this paper, we only consider the net aberration contribution of misalignments, and therefore, the first component in Eq. (7) is neglected. In addition, considering that the magnitude of misalignments is typically very small, the third component can also be neglected for misalignment-level perturbations. When only the third-order aberrations of the on-axis parent system are considered, the analytics expressions for the net astigmatic and coma aberration contributions of a certain set of lateral misalignments are presented in Eqs. (9) and (10), respectively, i.e.,

$$\Delta W_{\mathrm{AST}} = -(\Delta\vec{A}_{222}\vec{H} + \vec{s}\Delta\vec{A}_{131}) \cdot \vec{\rho}^2, \qquad (9)$$

$$\Delta W_{\mathrm{Coma}} = -\Delta\vec{A}_{131} \cdot [\vec{\rho}(\vec{\rho} \cdot \vec{\rho})], \qquad (10)$$

where Δ indicates the related variables are net changes induced by a certain set of lateral misalignments, which are introduced into an off-axis telescope. Note that in general an expression that contains $\vec{A}_{131}$ or $\vec{A}_{222}$ describes a misalignment-induced change. The reason for us to use a "Δ" is that $\vec{A}_{131}$ and $\vec{A}_{222}$ usually are related to the aberration contributions of the total misalignments of system. However, in some cases, we only care the net aberration contributions of the net changes in the misalignment parameters. In practice and in our experiment, we do not know the specific misalignments of the system, and we can only determine the change in misalignment parameters (by introducing a known set of misalignments to the system). Therefore, Eqs. (9) and (10) are mainly used to describe the net changes of aberrations due to the net changes in misalignment parameters. If the optical system is in the nominal state before we introduce misalignments into it, then Δ can be neglected.

We can see that the misalignment-induced astigmatism contains two components, i.e., a field-linear component and field-constant component. The misalignment-induced coma only contains a field-constant component. In addition, we can see that the expression of the field-constant astigmatism and field-constant coma both contain the vector $\vec{A}_{131}$. This indicates that, in pupil-offset off-axis telescopes, these two dominate kinds of misalignment-induced aberrations have some inherent relations. The inherent relations between the magnitude and orientation of astigmatism and coma induced by lateral misalignments can be roughly expressed as Eqs. (11) and (12),[19] respectively, i.e.,

$$|\Delta\vec{C}_{5/6}| = 3|\vec{s}| \cdot |\Delta\vec{C}_{7/8}|, \qquad (11)$$

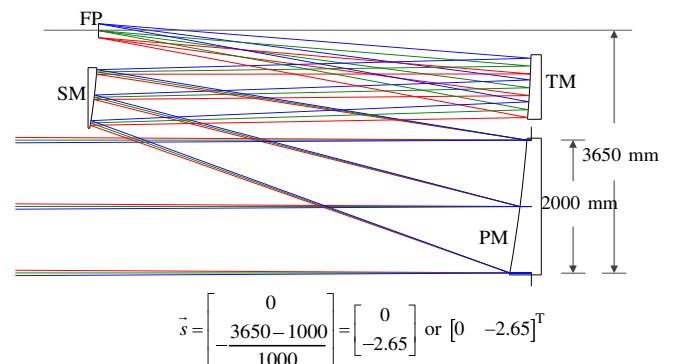$$2\phi_{\Delta W_{\mathrm{AST}}} = \phi_{\Delta W_{\mathrm{Coma}}} + \xi(\vec{s}), \qquad (12)$$

where $|\Delta\vec{C}_{5/6}| \equiv \sqrt{(\Delta C_5)^2 + (\Delta C_6)^2}$, representing the magnitude of the field-constant component of the misalignment-induced astigmatism, and C_i is i'th fringe Zernike coefficient. Here, $|\Delta\vec{C}_{7/8}| \equiv \sqrt{(\Delta C_7)^2 + (\Delta C_8)^2}$, representing the magnitude of the misalignment-induced coma, $|\vec{s}|$ is the magnitude of the pupil decenter vector, $\xi(\vec{s})$ represents the azimuthal angle of the vector $\vec{s}$, and $\phi_{\Delta W_{\mathrm{AST}}}$ and $\phi_{\Delta W_{\mathrm{Coma}}}$ represent the orientation of the misalignment-induced astigmatism and coma, respectively. The underlying reason for this is that the field-constant astigmatism is mainly attributed to the effects of pupil offset, which converts the on-axis coma to off-axis astigmatism.

3 Simulations

3.1 Illustration of the Misalignment-Induced Astigmatic and Coma Aberration Fields in Misaligned Off-Axis Three-Mirror Anastigmatic Telescopes

To illustrate the astigmatic and coma aberration fields presented above, an off-axis TMA telescope suitable for space application designed by Moretto et al.[24] is used, which was once a preliminary off-axis optical configuration for the Supernova/Acceleration Probe (SNAP) Mission. This aperture size of the primary mirror (PM) is 2 m and the F number is 10. The optical layout of this telescope is presented in Fig. 2 and the optical design parameters are presented in Appendix B. In Fig. 2, we can see that the specific value of the normalized pupil decentration vector $\vec{s}$ is $[0 \quad -2.65]^{\mathrm{T}}$.

In this section, the full-field displays (FFDs) of CODE V® are used to demonstrate the astigmatic and coma aberration

$$\vec{s} = \begin{bmatrix} 0 \\ -\dfrac{3650-1000}{1000} \end{bmatrix} = \begin{bmatrix} 0 \\ -2.65 \end{bmatrix} \text{ or } [0 \quad -2.65]^{\mathrm{T}}$$

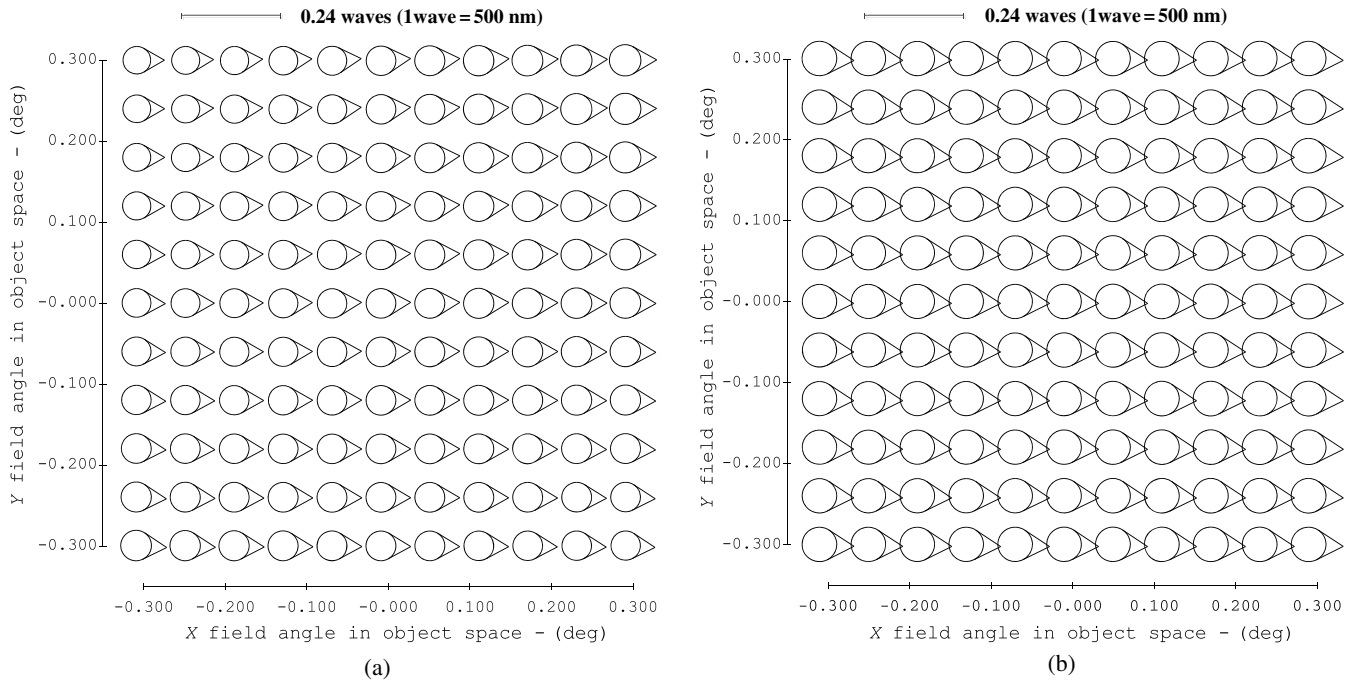**Fig. 2** Optical layout of the off-axis SNAP telescope.

Fig. 3 FFDs for (a) coma (Z7/Z8) in the off-axis SNAP telescope and (b) its parent on-axis telescope with the same aperture size in the presence of the same lateral misalignments.

fields induced by lateral misalignments. The FFDs over a moderate field of view (±0.3 deg) for the misalignment-induced coma (Z7/Z8) and astigmatism (Z5/Z6) of this off-axis telescope and its parent telescope with the same aperture size are shown in Figs. 3 and 4, respectively. The misalignment parameters are the same for Figs. 3 and 4, which are shown in Table 2.

In Table 2, XDE and BDE represent the mirror vertex decenter and tip–tilt in the x–z plane, respectively. YDE and ADE represent the mirror vertex decenter and tip–tilt in the y–z plane, respectively.

Note that for TMA telescopes, the third-order aberrations are corrected in the nominal state and we can neglect them in our discussions. Therefore, we can roughly consider the total aberrations in the presence of misalignments as the aberrations induced by misalignments. It can be seen from Fig. 3 that misalignment-induced coma in the off-axis TMA telescope is
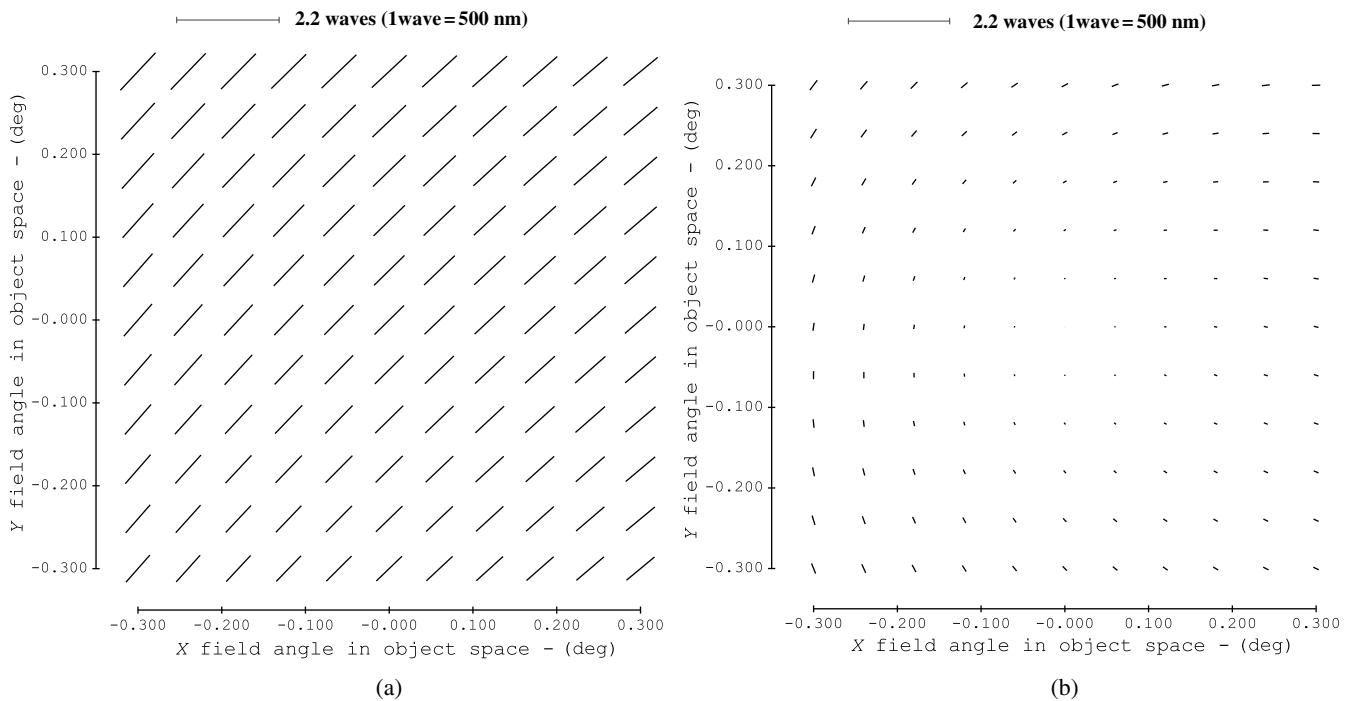

Fig. 4 FFDs for (a) astigmatism (Z5/Z6) in the off-axis SNAP telescope and (b) its parent on-axis telescope with the same aperture size in the presence of the same lateral misalignments.

Table 2 The specific misalignment parameters for Figs. 3 and 4.

Mirror	XDE (mm)	YDE (mm)	ADE (deg)	BDE (deg)
SM	0.30	0.10	0.008	0.020
TM	0.07	0.05	−0.005	−0.008

similar with that in the on-axis telescope, both of which are field constant. Considering that the misalignment-induced coma in on-axis telescopes can be accurately represented by Eq. (10),[2] therefore, the coma aberration field induced by misalignments in off-axis TMA telescopes can still be roughly represented by Eq. (10).

On the other hand, it can be seen from Fig. 4 that the misalignment-induced astigmatism in the off-axis TMA telescope is very different from that in the on-axis telescope. Specifically, the astigmatic aberration field in the off-axis TMA telescope induced by lateral misalignments can be seen as a combination of a field-linear, field-asymmetric term, which is exactly the astigmatic term that exists in misaligned on-axis TMA telescopes and a larger field-constant term. Through Eq. (9), we can recognize that this field-constant term is mainly attributed to the effects of pupil offset, which converts the on-axis coma to the off-axis astigmatism.

In addition, considering that the misalignment parameters are the same for Figs. 3 and 4, the inherent relationships between the magnitude and orientation of coma and astigmatism expressed by Eqs. (11) and (12) can be illustrated with Figs. 3(a) and 4(a). On one hand, the ratio of the magnitude of astigmatism to the magnitude of coma is about 9, which is close to $3|\vec{s}|$ (the value of $3|\vec{s}|$ is approximately equal to 8). On the other hand, the direction of coma in Fig. 3(a) is about π, and we can obtain that the direction of astigmatism is about $\pi/4$ according to Eq. (12), which is in accordance with Fig. 4(a).

3.2 Nodal Property of the Astigmatic Aberration Field in Misaligned Off-Axis Three-Mirror Anastigmatic Telescopes

Considering that the astigmatic aberration field in misaligned off-axis TMA telescopes is very different from that in on-axis ones, this section presents some discussions about nodal property of this misalignment-induced aberration field to provide a better understanding of it.

For TMA telescopes, all the third-order aberrations can be corrected. In this case, we can neglect the aberrations of the nominal system and only consider those induced by misalignments represented by Eq. (9), which can further be rewritten as

$$\Delta W_{\text{AST}} = -\vec{A}_{222}\left[\vec{H} - \left(-\frac{\vec{A}_{131}\vec{s}}{\vec{A}_{222}}\right)\right] \cdot \vec{\rho}^2, \quad \text{if } \vec{A}_{222} \neq \vec{0}. \quad (13)$$

From this perspective, we can consider that the astigmatism in off-axis TMA telescopes with lateral misalignments is still field-linear and field-asymmetric, which is similar to the misalignment astigmatism in on-axis TMA telescopes.[2] However, it is important to recognize that the node of this field-linear, field-asymmetric astigmatism has been shifted to $-\frac{\vec{A}_{131}^{(P)}\vec{s}}{\vec{A}_{222}^{(P)}}$, no longer located at the field center. In addition, in the following,

we show that this node is generally not located in the field of view, either. In Eq. (13), we remove the symbol Δ. As mentioned before, Δ is used to represent the changes in aberrations due to the changes in misalignment parameters. If the optical system is in the nominal state before we introduce misalignments, then the changes in misalignment parameters are equivalent to the total misalignments. In this case, we can remove the symbol Δ for simplicity.

According to the Seidel formula, for on-axis systems, we have

$$W_{222j}^{\text{(sph)}} = \frac{\bar{i}_j}{i_j} W_{131j}^{\text{(sph)}}, \qquad W_{222j}^{\text{(asph)}} = \frac{\bar{y}_j}{y_j} W_{131j}^{\text{(asph)}}, \qquad (14)$$

where the superscripts (sph) and (asph) indicate that these aberration coefficients are for the spherical base sphere and the aspheric departure, respectively, $\bar{i}_j$ and i_j are the chief-ray incident angle and marginal-ray incident angle at surface j, respectively, and $\bar{y}_j$ and y_j are the chief-ray height and marginal-ray height at the surface j, respectively. In general, for the mirrors in large astronomical telescope systems with a moderate field of view, especially PM and secondary mirror (SM), we can have $|\bar{i}_j| < |i_j|$, $|\bar{y}_j| < |y_j|$ (here, $|\cdot|$ represents the absolute value operator). Referring to Eq. (14), we can know that the coma aberration coefficient for an individual surface is usually much larger than astigmatic aberration coefficient, which indicates that the magnitude $|\vec{A}_{131}|$ is usually much larger than the magnitude $|\vec{A}_{222}|$. In addition, for off-axis TMA telescopes with unobscured pupils, we at least have $|\vec{s}| > 1$ and usually $|\vec{s}|$ is about 2 ($|\vec{s}|$ represents the ratio of the pupil displacement to the half pupil size). Consequently, in general, we can have

$$\left|-\frac{\vec{A}_{131}\vec{s}}{\vec{A}_{222}}\right| = \frac{|\vec{A}_{131}|}{|\vec{A}_{222}|} \cdot |\vec{s}| > 1, \qquad (15)$$

which indicates that the node of this field-linear, field-asymmetric astigmatism in misaligned off-axis TMA telescopes usually lies outside of (and far away from) the field of view.

The underlying reason for this is that the magnitude of the coma is magnified when it is converted into astigmatism through pupil coordinate transformation. This larger field-constant astigmatism term will displace the node from field center to some position out of the field of view. This conclusion can be partly demonstrated by Fig. 4(a). On the other hand, we should note that $|\vec{A}_{131}|$ is not always larger than $|\vec{A}_{222}|$. In the case where the misalignment of a mirror can be seen as a rotation of the mirror about its coma-free pivot point, no additional coma will be introduced into the system.

4 Experiment

4.1 Experiment Setup

In this section, an experiment is performed to further validate the correctness of the extension of nodal aberration theory to pupil-offset off-axis telescopes. A real off-axis TMA telescope with an offset pupil is used here; the specifications of this telescope are presented in Table 3.

The schematic and physical maps of the experimental setup with the off-axis TMA telescope are shown in Figs. 5 and 6, respectively.

Table 3 The specifications of the off-axis TMA telescope.

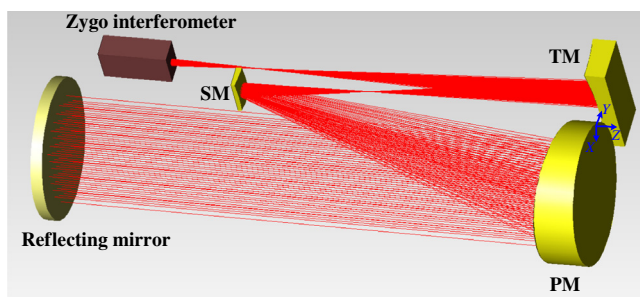| Parameter	Value
Aperture	500 mm
Aperture offset	−460 mm
Wavelength	632.8 nm
Focal length	6000 mm
Field of view	1.1 deg × 0.25 deg
Field offset	−0.3 deg

Fig. 5 The schematic of the experimental setup.

Specifically, the interferometer, flat reflecting mirror, and the off-axis TMA telescope form a self-collimation optical path for detecting the aberrations of the system. The whole experiment setup is placed on an air-bearing platform to suppress the effects of vibration on the detection results. The PM serves as the coordinate reference, and we use a mask to accurately control its actual aperture size. The SM is placed on a high-precision hexapod (PI instrumental, Model C-887) that can control SM to align the system or purposely introduce misalignments to the system (the hexapod has six degrees of freedom). The rotational center of the SM has been carefully determined to be in accordance with definition of CODE V®. The tertiary mirror (TM) is placed on a fine five-dimensional adjustment frame for alignment. Two dial gauges are used to monitor the decenter of the TM in two directions (there is another dial gauge located behind the TM,

which is not shown in Fig. 6). The flat reflecting mirror is used for wavefront measurements at multiple field positions, and the pose (i.e., azimuthal angle and pitching angle) of it can be precisely controlled with a theodolite and a two-dimensional (can only be rotated and not be translated) adjustment frame. A row of fans is utilized to disturb the temperature field in the room and make the temperature distribution more uniform. Otherwise, the difference between the temperatures of the cold platform below the optical system and the warm air above the optical system can make the refractive index of the air nonuniform, resulting in measurement errors (this nonuniformity changes gradually, making it hard to calibrate). We will repeat the measurement process thousands of times with interferometer and take the average value.

The off-axis TMA telescope was first assembled and then roughly aligned. Since in this paper we concentrate on the net aberration fields induced by lateral misalignments, not the nominal aberration fields, we do not pursue the perfect alignment state of the system.

4.2 *Experiment Procedure and Result Analysis*

When the alignment process of off-axis TMA telescope is roughly completed, we can begin to perform the experiment for demonstrating the correctness of the extension of nodal aberration theory to off-axis TMA telescopes. The specific experiment procedure is presented below:

1. Measure the wavefront aberration coefficients of the off-axis TMA telescope at five field points with the interferometer. The specific positions of the five field points are presented in Fig. 7 (red points). Before wavefront measurement at each field point, the azimuthal and pitching angle of the flat mirror that is monitored by a theodolite should be accurately adjusted.

2. Introduce two known sets of lateral misalignments into the off-axis TMA telescope, the specific values of which are shown in Table 4. In case 1, an additional set of SM misalignments is introduced with hexapod. In case 2, apart from SM misalignments, an additional set of TM misalignments is also introduced with adjustment frame, under the monitor of dial gauges
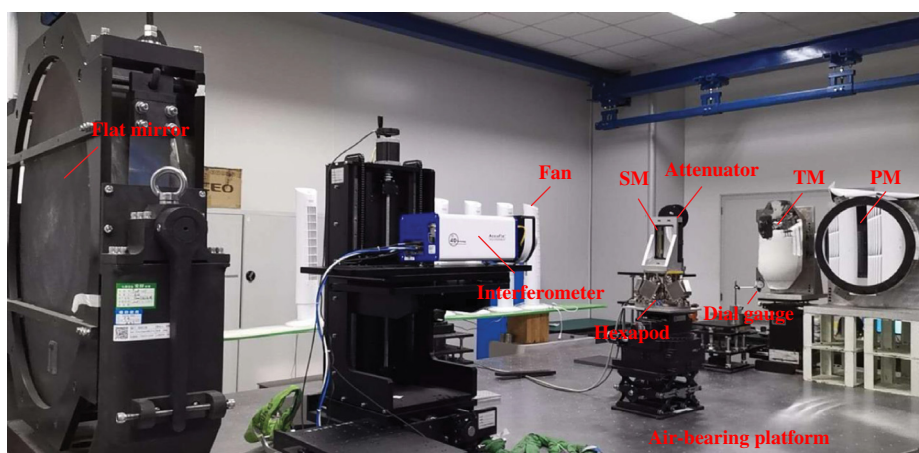

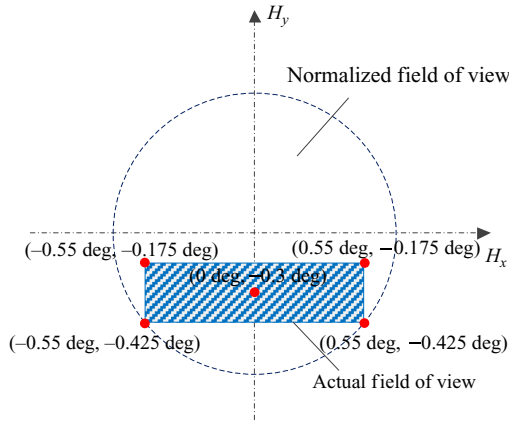**Fig. 6** The physical map of the experimental setup.

Fig. 7 The positions of the five targeted points in the field.

Table 4 The intentionally introduced misalignment parameters in the two cases.

		ΔXDE (mm)	ΔYDE (mm)	ΔADE (deg)	ΔBDE (deg)
Case 1	SM	0.3	−0.3	0.01	0.01
	TM	0	0	0	0
Case 2	SM	−0.3	0.3	−0.01	−0.01
	TM	1	1	0	0

(the changes in the tip–tilts of TM are hard to monitor, and therefore we, here, only introduce decenters of the TM). In Table 4, Δ indicates that these misalignments are net change values, not absolute misalignment values.

3. Measure the wavefront aberration coefficients of the off-axis TMA telescope at the five field points with interferometer again for each of the misalignment cases, and compute the net changes of the aberration coefficients at each field point induced by the intentionally introduced misalignments.

4. Theoretically compute the net aberration contribution of the intentionally introduced misalignments using Eqs. (9) and (10) for each of the misalignment cases. Meanwhile, the shifts of the aberration field center of SM and TM (including $\Delta\vec{\sigma}_{SM}^{(sph)}$, $\Delta\vec{\sigma}_{SM}^{(asph)}$, $\Delta\vec{\sigma}_{TM}^{(sph)}$, and $\Delta\vec{\sigma}_{TM}^{(asph)}$) can be computed according to Ref. 22.

5. Compare the results of analytical expressions with those obtained through real experiment and analyze the deviations between them. If the results of analytical expressions are approximately equal to the experimental results, the correctness of the extension of nodal aberration theory to off-axis TMA telescopes can be validated.

The wavefront maps of the off-axis TMA telescope at the five designated field positions before introducing misalignments to the system are shown in Fig. 8(a). Wavefront maps after

introducing the two sets of misalignments (shown in Table 5) into the system are shown in Figs. 8(b) and 8(c), respectively.

We can see from Fig. 8(a) that the system has some high-order components in the wavefront map due to figure degeneration of the PM and TM, especially TM, for we can recognize that the effects of figure error are field dependent. After introducing one set of misalignments into the system, the effects of figure error are submerged by the effects of misalignments. It can be seen from Figs. 8(b) and 8(c) that the effects of lateral misalignments are nearly field constant (mainly astigmatism), and it is hard to distinguish between the wavefront maps at different fields.

The net changes of the astigmatic and coma aberration coefficients at the five designated field positions induced by the two sets of intentionally introduced misalignments are shown in Table 5, including those actually measured aberration coefficients and those analytically computed with Eqs. (9) and (10) (the relationships between Seidel aberration coefficients and fringe Zernike coefficients should be considered). Some discussions on Table 5 are shown below:

1. On one hand, it can be seen that the actually measured aberration coefficients and those analytically computed are roughly in accordance. The mean deviation between the analytically computed coefficients and those actually measured is 0.0185λ for case 1 and 0.0161λ for case 2. They also represent similar aberration field characteristics. Specifically, the misalignment-induced astigmatism contains a dominant field-constant component and smaller field-linear component, and the misalignment-induced coma is nearly field constant.

2. On the other hand, there still exist some deviations between them, and on the whole, we can roughly recognize that the magnitudes of the analytically computed aberration coefficients are a little smaller than those actually measured, which indicates a systematic error. The main reason that may result in these deviations (except those random measurement errors induced by environmental perturbations) is that we neglect the aberration contributions of the misalignment-induced higher-order aberrations [such as $\vec{A}_{151} \cdot \vec{\rho}(\vec{\rho} \cdot \vec{\rho})$ or $\vec{A}_{171} \cdot \vec{\rho}(\vec{\rho} \cdot \vec{\rho})$] of the on-axis parent system in the derivation of Eqs. (9) and (10). As presented in Ref. 19, these aberrations can generate astigmatism and coma through pupil coordinate transformation, and the magnitudes of astigmatism and coma generated by them are usually far larger than the magnitudes of themselves, in spite that the magnitudes of them are usually very small.

3. In addition, we should note that the system is not in perfect alignment state before additionally introducing misalignments. The initial wavefront aberrations can have a negative or positive effect on the final wavefront of the system after introducing additional misalignment to the system. This is the main reason for why the net changes of aberration coefficients in case 2 are larger than case 1 while the final RMS wavefront error in Fig. 8(c) is smaller than Fig. 8(b) for several field points.
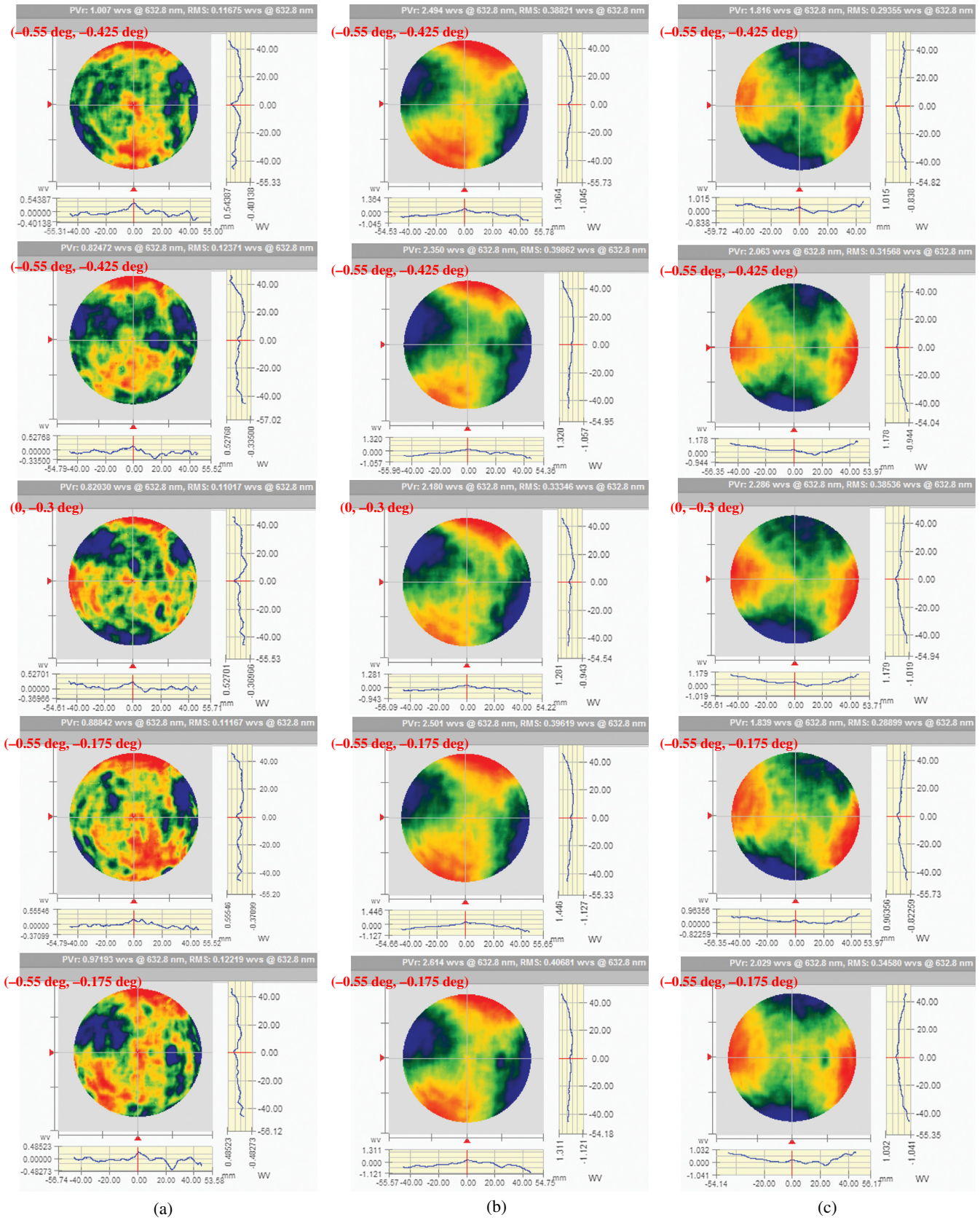
Fig. 8 One set of wavefront maps for the off-axis TMA telescope at the five designated field positions (a) before introducing misalignments and after introducing two different sets of misalignments to the system, which correspond to (b) case 1 and (c) case 2 as shown in Table 4, respectively.

Table 5 The comparisons between the actually measured fringe Zernike aberration coefficients (A) and those analytically computed (B) induced by misalignments for the two misalignment cases shown in Table 4.

Coefficient type	Field position	Case 1		Case 2	
		A	B	A	B
ΔC_5	(−0.55 deg, −0.425 deg)	0.505	0.520	−0.709	−0.723
	(0.55 deg, −0.425 deg)	0.621	0.659	−0.877	−0.901
	(0 deg, −0.3 deg)	0.544	0.605	−0.786	−0.823
	(−0.55 deg, −0.175 deg)	0.527	0.552	−0.692	−0.745
	(0.55 deg, −0.175 deg)	0.635	0.690	−0.889	−0.923
ΔC_6	(−0.55 deg, −0.425 deg)	0.635	0.659	−0.369	−0.416
	(0.55 deg, −0.425 deg)	0.496	0.520	−0.300	−0.318
	(0 deg, −0.3 deg)	0.567	0.605	−0.370	−0.387
	(−0.55 deg, −0.175 deg)	0.659	0.690	−0.405	−0.458
	(0.55 deg, −0.175 deg)	0.521	0.552	−0.354	−0.358
ΔC_7	(−0.55 deg, −0.425 deg)	−0.118	−0.117	0.067	0.079
	(0.55 deg, −0.425 deg)	−0.104	−0.117	0.076	0.079
	(0 deg, −0.3 deg)	−0.113	−0.117	0.065	0.079
	(−0.55 deg, −0.175 deg)	−0.112	−0.117	0.059	0.079
	(0.55 deg, −0.175 deg)	−0.096	−0.117	0.073	0.079
ΔC_8	(−0.55 deg, −0.425 deg)	0.095	0.117	−0.152	−0.154
	(0.55 deg, −0.425 deg)	0.103	0.117	−0.139	−0.154
	(0 deg, −0.3 deg)	0.099	0.117	−0.144	−0.154
	(−0.55 deg, −0.175 deg)	0.106	0.117	−0.133	−0.154
	(0.55 deg, −0.175 deg)	0.112	0.117	−0.126	−0.154

Note: Fringe Zernike coefficients are in $\lambda(\lambda = 632.8$ nm).

Note that in the optical simulation software, such as CODE V®, the symmetry plane of the off-axis system is usually in the vertical direction, whereas in our experimental setup, the symmetry plane of the off-axis system is in the horizontal direction, as shown in Fig. 6. Therefore, some coordinate transformations between the coordinate system of the interferometer and the optical model in CODE V® should be implemented to convert the measured wavefront aberration coefficients to the actual aberration coefficients of optical model in CODE V, for our theoretical calculations are based on the coordinate system of CODE V. In addition, the mask needed in wavefront measurement using interferometer should be carefully determined.

Then we continue to demonstrate the inherent relations between the field-constant astigmatism component and the field-constant coma, which are induced by lateral misalignment. These relations are deduced from the extension of nodal aberration theory to off-axis systems. Therefore, if these relations can be validated through experiment, the correctness of the extension of nodal aberration theory to off-axis systems can

further be validated. The specific validation processes are presented in Table 6. The measured aberration coefficients presented in Table 5 are first fitted with Eqs. (9) and (10). The fitted expressions for the net astigmatism and coma aberration are shown in the first two lines in Table 6. The magnitudes and azimuth angles of them [we can refer to Eq. (44) of Ref. 19 for the computation of these azimuth angles] are shown in this table. The last two lines present the last validation procedures for the inherent relations between the net astigmatism and coma induced by lateral misalignments for the two cases.

We can see from the last two lines in Table 6 that the inherent relationships revealed in the experimental data are roughly in accordance to the analytic expressions shown in Eqs. (11) and (12). (We can neglect the additional 2π shown in the last rows, for 2π is the period of the angles.) These results validate the inherent relations between astigmatism and coma induced by lateral misalignments, which are nearly independent of the specific values of the lateral misalignments (but dependent on the specific kind of misalignments).[20]

Table 6 Validation processes for the inherent relations between the net astigmatism and coma induced by lateral misalignments for the two cases.

	Case 1	Case 2
ΔW_{AST}	$\left(\begin{bmatrix} 0.0711 \\ -0.0863 \end{bmatrix} \vec{H} + \begin{bmatrix} 0.6034 \\ 0.6061 \end{bmatrix}\right) \cdot \vec{\rho}^2$	$\left(\begin{bmatrix} -0.1166 \\ 0.0360 \end{bmatrix} \vec{H} + \begin{bmatrix} -0.8060 \\ -0.4096 \end{bmatrix}\right) \cdot \vec{\rho}^2$
ΔW_{Coma}	$\begin{bmatrix} -0.1086 \\ 0.1030 \end{bmatrix} \cdot 3\vec{\rho}(\vec{\rho} \cdot \vec{\rho})$	$\begin{bmatrix} 0.0680 \\ -0.1388 \end{bmatrix} \cdot 3\vec{\rho}(\vec{\rho} \cdot \vec{\rho})$
$\|\Delta\vec{C}_{5/6}\|$	$\sqrt{0.6034^2 + 0.6061^2} = 0.8552$	$\sqrt{0.8060^2 + 0.4096^2} = 0.9041$
$\|\Delta\vec{C}_{7/8}\|$	$\sqrt{0.1086^2 + 0.1030^2} = 0.1497$	$\sqrt{0.0680^2 + 0.1388^2} = 0.1546$
$2\phi_{\Delta W_{\text{AST}}}$	$\tan^{-1}\left(\frac{0.6061}{0.6034}\right) = 0.7806$	$\pi + \tan^{-1}\left(\frac{0.4096}{0.8060}\right) = 3.6118$
$\phi_{\Delta W_{\text{Coma}}}$	$\pi + \tan^{-1}\left(-\frac{0.1030}{0.1086}\right) = 2.3827$	$2\pi + \tan^{-1}\left(-\frac{0.1388}{0.0680}\right) = 5.1679$
$\|\Delta\vec{C}_{5/6}\| - 3\|\vec{s}\| \cdot \|\Delta\vec{C}_{7/8}\|$	$0.8552 - 3 \cdot \frac{460}{250} \cdot 0.1497 = 0.0289$	$0.9041 - 3 \cdot \frac{460}{250} \cdot 0.1546 = 0.0507$
$2\phi_{\Delta W_{\text{AST}}} - [\phi_{\Delta W_{\text{Coma}}} + \xi(\vec{s})]$	$0.7806 - \left(2.3827 + \frac{3\pi}{2}\right) = -0.0313 - 2\pi$	$3.6118 - \left(5.1679 + \frac{3\pi}{2}\right) = 0.0147 - 2\pi$

Note: Magnitudes of aberrations are in $\lambda (\lambda = 632.8 \text{ nm})$ and the azimuth angles of them are in rad.

5 Conclusion

This work presents an experimental study for the extension of nodal aberration theory to pupil-offset off-axis telescopes for the first time. While the traditional nodal aberration theory can be utilized well to analytically describe the misalignment aberration field characteristics of on-axis telescopes, it is not directly applicable to pupil-offset off-axis telescopes. The net aberration field characteristics of off-axis TMA telescopes induced by lateral misalignments are still not well-known in field of optics. In this paper, nodal aberration theory is extended to off-axis telescopes with a pupil coordinate transformation. The astigmatism and coma aberration fields as well as their inherent relations are analytically expressed, simulated, and quantitatively validated with real off-axis TMA telescope. It is shown that the experimental results are approximately in accordance with the analytic expressions. In addition, the deep discussions about the differences between the misalignment aberrations of on-axis and off-axis TMA telescopes contribute to a better understanding of the effects of lateral misalignments on the aberration fields of off-axis TMA telescopes.

6 Appendix A: Derivations for the Specific Expressions of $\vec{C}_{lm}^{(0)}$, $\vec{C}_{lm}^{(1)}$, and $\sum_{i=2}^{\infty} \vec{C}_{lm}^{(i)}$.

When only the third-order aberrations of the on-axis parent system are considered, Eq. (5) can be written as

$$W = \sum_j W_{220Mj}(\vec{H}_{Aj} \cdot \vec{H}_{Aj})[(\vec{\rho} + \vec{s}) \cdot (\vec{\rho} + \vec{s})]$$

$$+ \frac{1}{2}\sum_j W_{222j}[\vec{H}_{Aj}^2 \cdot (\vec{\rho} + \vec{s})^2]$$

$$+ \sum_j W_{131j}[\vec{H}_{Aj} \cdot (\vec{\rho} + \vec{s})][(\vec{\rho} + \vec{s}) \cdot (\vec{\rho} + \vec{s})]$$

$$+ \sum_j W_{040j}[(\vec{\rho} + \vec{s}) \cdot (\vec{\rho} + \vec{s})]^2, \qquad (16)$$

where $W_{220Mj} = W_{220j} + 1/2W_{222j}$,[9] representing the coefficient for medial focal surface. Equation (16) can be expanded as

$$W = \sum_j W_{220Mj}[(\vec{H}_{Aj} \cdot \vec{H}_{Aj})(\vec{\rho} \cdot \vec{\rho}) + 2(\vec{H}_{Aj} \cdot \vec{H}_{Aj})(\vec{s} \cdot \vec{\rho})$$

$$+ (\vec{H}_{Aj} \cdot \vec{H}_{Aj})(\vec{s} \cdot \vec{s})]$$

$$+ \frac{1}{2}\sum_j W_{222j}[\vec{H}_{Aj}^2 \cdot \vec{\rho}^2 + 2\vec{H}_{Aj}^2\vec{s}^* \cdot \vec{\rho} + \vec{H}_{Aj}^2 \cdot \vec{s}^2]$$

$$+ \sum_j W_{131j}\begin{bmatrix} (\vec{H}_{Aj} \cdot \vec{\rho}) \cdot (\vec{\rho} \cdot \vec{\rho}) + 2(\vec{s} \cdot \vec{s})(\vec{H}_{Aj} \cdot \vec{\rho}) + \vec{H}_{Aj}\vec{s} \cdot \vec{\rho}^2 \\ + 2(\vec{H}_{Aj} \cdot \vec{s})(\vec{\rho} \cdot \vec{\rho}) + \vec{s}^2\vec{H}_{Aj}^* \cdot \vec{\rho} + (\vec{s} \cdot \vec{s})(\vec{H}_{Aj} \cdot \vec{s}) \end{bmatrix}$$

$$+ \sum_j W_{040j}\begin{bmatrix} (\vec{\rho} \cdot \vec{\rho})^2 + 4(\vec{s} \cdot \vec{s})(\vec{\rho} \cdot \vec{\rho}) + 2\vec{s}^2 \cdot \vec{\rho}^2 + \\ 4(\vec{s} \cdot \vec{\rho})(\vec{\rho} \cdot \vec{\rho}) + 4(\vec{s} \cdot \vec{s})(\vec{s} \cdot \vec{\rho}) + (\vec{s} \cdot \vec{s})^2 \end{bmatrix}. \qquad (17)$$

In this expansion, the following two vector multiplication identities are needed:

$$\vec{A} \cdot \vec{B}\,\vec{C} = \vec{A}\vec{B}^* \cdot \vec{C}, \qquad (18)$$

$$2(\vec{A} \cdot \vec{B})(\vec{C} \cdot \vec{B}) = (\vec{A} \cdot \vec{C})(\vec{B} \cdot \vec{B}) + \vec{A}\,\vec{C} \cdot \vec{B}^2. \qquad (19)$$

Equation (17) can further be rewritten as

$$W = \left[\sum_j W_{220Mj}(\vec{H}_{Aj} \cdot \vec{H}_{Aj}) + 2\sum_j W_{131j}(\vec{H}_{Aj} \cdot \vec{s}) \right.$$
$$\left. + 4\sum_j W_{040j}(\vec{s} \cdot \vec{s}) \right](\vec{\rho} \cdot \vec{\rho})$$
$$+ \left(\frac{1}{2}\sum_j W_{222j}\vec{H}_{Aj}^2 + \sum_j W_{131j}\vec{H}_{Aj}\vec{s} + 2\sum_j W_{040j}\vec{s}^2 \right) \cdot \vec{\rho}^2$$
$$+ \left(4\sum_j W_{040j}\vec{s} + \sum_j W_{131j}\vec{H}_{Aj} \right) \cdot \vec{\rho}(\vec{\rho} \cdot \vec{\rho})$$
$$+ \sum_j W_{040j}(\vec{\rho} \cdot \vec{\rho})^2, \tag{20}$$

where the aberration terms are regrouped according to their pupil dependence and the tip–tilt and piston terms are neglected. By substituting Eq. (3) into Eq. (20), we can obtain

$$W = \left\{ \begin{array}{l} [W_{220M}(\vec{H} \cdot \vec{H}) + 2W_{131}(\vec{s} \cdot \vec{H}) + 4W_{040}(\vec{s} \cdot \vec{s})] \\ +(-2\vec{A}_{220M} \cdot \vec{H} - 2\vec{A}_{131} \cdot \vec{s}) + \sum_j W_{220M}(\vec{\sigma}_j \cdot \vec{\sigma}_j) \end{array} \right\}$$
$$\cdot (\vec{\rho} \cdot \vec{\rho}) + \left[\begin{array}{l} \left(\frac{1}{2}W_{222}\vec{H}^2 + W_{131}\vec{s}\vec{H} + 2W_{040}\vec{s}^2 \right) + \\ (-\vec{A}_{222}\vec{H} - \vec{A}_{131}\vec{s}) \cdot \vec{\rho}^2 + \left(\sum_j W_{222}\vec{\sigma}_j^2 \right) \end{array} \right]$$
$$\cdot \vec{\rho}^2 + [(W_{131}\vec{H} + 4W_{040}\vec{s}) + (-\vec{A}_{131})] \cdot \vec{\rho}(\vec{\rho} \cdot \vec{\rho})$$
$$+ (W_{040}) \cdot (\vec{\rho} \cdot \vec{\rho})^2. \tag{21}$$

For simplicity, W_{020} term is not included in the above derivation.

7 Appendix B: Optical Design Parameters of the Off-Axis SNAP Telescope

The basic optical parameters of the off-axis SNAP telescope are shown in Table 7, and its high-order aspheric parameters are shown in Table 8.

Table 7 The basic optical parameters of the off-axis SNAP telescope.

Surface	Radius (mm)	Conic	Thickness (mm)
PM (stop)	−20744.807	−0.9601	−6464.181
SM	−8551.657	0.0000	6464.181
TM	−15497.513	0.0000	−6464.181

Table 8 The aspheric parameters of the off-axis SNAP telescope.

Surface	Fourth order	Sixth order	Eighth order	Tenth order
PM (stop)	5.286×10^{-15}	2.570×10^{-24}	0	0
SM	5.197×10^{-13}	-1.672×10^{-21}	5.704×10^{-29}	-2.097×10^{-36}
TM	7.093×10^{-14}	-5.336×10^{-24}	0	0

References

1. T. Schmid, K. P. Thompson, and J. P. Rolland, "Misalignment-induced nodal aberration fields in two-mirror astronomical telescopes," *Appl. Opt.* **49**(16), D131–D144 (2010).
2. K. P. Thompson, T. Schmid, and J. P. Rolland, "The misalignment induced aberrations of TMA telescopes," *Opt. Express* **16**(25), 20345–20353 (2008).
3. H. H. Hopkins, *The Wave Theory of Aberrations*, Oxford on Clarendon Press (1950).
4. R. A. Buchroeder, "Tilted component optical systems," PhD Dissertation, University of Arizona, Tucson, Arizona (1976).
5. R. V. Shack and K. P. Thompson, "Influence of alignment errors of a telescope system on its aberration field," *Proc. SPIE* **251**, 146–153 (1980).
6. D. Hestenes, "Oersted Medal Lecture 2002: reforming the mathematical language of physics," *Am. J. Phys.* **71**(2), 104–121 (2003).
7. W. K. Clifford, "Applications of Grassmann's extensive algebra," *Am. J. Math.* **1**, 350–358 (1878).
8. K. P. Thompson, "Aberration fields in tilted and decentered optical systems," PhD Dissertation, University of Arizona, Tucson, Arizona (1980).
9. K. Thompson, "Description of the third-order optical aberrations of near-circular pupil optical systems without symmetry," *J. Opt. Soc. Am. A* **22**(7), 1389–1401 (2005).
10. K. P. Thompson, "Multinodal fifth-order optical aberrations of optical systems without rotational symmetry: spherical aberration," *J. Opt. Soc. Am. A* **26**(5), 1090–1100 (2009).
11. K. P. Thompson, "Multinodal fifth-order optical aberrations of optical systems without rotational symmetry: the comatic aberrations," *J. Opt. Soc. Am. A* **27**(6), 1490–1504 (2010).
12. K. P. Thompson, "Multinodal fifth-order optical aberrations of optical systems without rotational symmetry: the astigmatic aberrations," *J. Opt. Soc. Am. A* **28**(5), 821–836 (2011).
13. J. M. Sasian, "Imagery of the bilateral symmetric optical system," PhD Dissertation, University of Arizona, Tucson, Arizona (1988).
14. J. Rogers, "Aberrations of unobscured reflective optical systems," PhD Dissertation, University of Arizona, Tucson, Arizona (1983).
15. J. Rogers, "Vector aberration theory and the design of off-axis systems," *Proc. SPIE* **554**, 76–81 (1985).
16. K. Fuerschbach, J. P. Rolland, and K. P. Thompson, "Extending nodal aberration theory to include mount-induced aberrations with application to freeform surfaces," *Opt. Express* **20**(18), 20139–20155 (2012).
17. K. Fuerschbach, J. P. Rolland, and K. P. Thompson, "Theory of aberration fields for general optical systems with freeform surfaces," *Opt. Express* **22**(22), 26585–26606 (2014).
18. N. Zhao et al., "Experimental investigation in nodal aberration theory (NAT) with a customized Ritchey–Chrétien system: third-order coma," *Opt. Express* **26**(7), 8729–8743 (2018).
19. G. Ju et al., "Aberration fields of off-axis two-mirror astronomical telescopes induced by lateral misalignments," *Opt. Express* **24**(21), 24665–24703 (2016).
20. G. Ju et al., "Nonrotationally symmetric aberrations of off-axis two-mirror telescopes induced by axial misalignments," *Appl. Opt.* **57**(6), 1399–1409 (2018).
21. G. Ju, H. Ma, and C. Yan, "Aberration fields of off-axis astronomical telescopes induced by rotational misalignments," *Opt. Express* **26**(19), 24816–24834 (2018).
22. K. P. Thompson et al., "Real-ray-based method for locating individual surface aberration field centers in imaging optical systems without rotational symmetry," *J. Opt. Soc. Am. A* **26**(6), 1503–1517 (2009).
23. J. Wang et al., "Third-order aberration fields of pupil decentered optical systems," *Opt. Express* **20**(11), 11652–11658 (2012).

24. G. Moretto, M. P. Langlois, and M. Ferrari, "Suitable off-axis space-based telescope designs," *Proc. SPIE* **5487**, 1111–1118 (2004).

Guohao Ju is a researcher at Changchun Institute of Optics, Fine Mechanics and Physics, Chinese Academy of Science. He is the first author of several journal papers published in OSA concerning the applications of nodal aberration theory. In particular, he presented for the first time a systematic discussion on the aberration fields of off-axis two-mirror astronomical telescopes by extending nodal aberration theory to include off-axis telescopes.

Hongcai Ma is a researcher at Changchun Institute of Optics, Fine Mechanics and Physics who majors in active optics and optical alignment.

Zhiyuan Gu is a researcher at Changchun Institute of Optics, Fine Mechanics and Physics who majors in optical design.

Changxiang Yan is a researcher at Changchun Institute of Optics, Fine Mechanics and Physics who majors in design and fabrication of optical instruments for remote sensing.